Quantitative X-ray Microanalysis

35

CHAPTER PREVIEW

You've now got an idea of how to acquire XEDS data from thin foils. You understand what factors may limit the information in them and what false and misleading effects may arise. Also, you know how to be sure that a certain peak is due to the presence of a certain element and the occasions when you may not be so sure. Having obtained a spectrum that is qualitatively interpretable, it turns out to be a remarkably simple procedure to convert that spectrum into quantitative data about the elements in your specimen, and this is what we describe in this chapter.

This chapter is rather long. You will find that you can skip parts of it as you work through it the first time. We have decided to keep the material together so as to be a more useful reference when you are actually doing the analysis on the microscope.

D. B. Williams et al., *Transmission Electron Microscopy*

Quantitative X-ray Microanalysis

35

35.1. HISTORICAL PERSPECTIVE

Quantitative X-ray analysis in the AEM is a most straightforward technique. What is surprising is that, given its simplicity, relatively few users take the trouble to extract quantitative data from their spectra, despite the fact that numerical data are the basis for all scientific investigations. Before we describe the steps for quantification, you should know a little about the historical development of quantitative X-ray microanalysis, because this will emphasize the advantages of thin-foil microanalysis over analysis of bulk specimens.

Historically, X-ray microanalysis in electron-beam instruments started with the study of bulk specimens in which the electron beam is totally absorbed, as opposed to "thin" specimens through which the beam penetrates. The possibility of using X-rays generated by a focused electron beam to give elemental information about the specimen was first described by Hillier and Baker (1944), and the necessary instrumentation was built several years later by Castaing (1951). In his extraordinary Ph.D. dissertation, Castaing not only described the equipment but also outlined the essential steps to obtain quantitative data from bulk specimens. The procedures that Castaing proposed still form the basis of the quantification routines used today in the EPMA and may be summarized as follows. Castaing assumed that the concentration C_i of an element i in the specimen generates a certain intensity of characteristic X-rays. However, it is very difficult in practice to measure this generated intensity so Castaing suggested that a known standard of composition $C_{(i)}$ be chosen for element i. We then measure the intensity ratio $I_i/I_{(i)}$, where I_i is the measured intensity emerging from (*not* generated within) the *specimen* and $I_{(i)}$ is the measured intensity emerging from the *standard*.

Castaing then proposed that, to a reasonable approximation

$$C_i / C_{(i)} = [K]\, I_i / I_{(i)} \qquad [35.1]$$

where K is a sensitivity factor that takes into account the difference between the generated and measured X-ray intensities for both the standard and the unknown specimen. The contributions to K come from three effects:

- Z The atomic number.
- A The absorption of X-rays within the specimen.
- F The fluorescence of X-rays within the specimen.

The correction procedure in bulk microanalysis is often referred to as the *ZAF* correction. The necessary calculations, which have been refined over the years since Castaing first outlined them, are exceedingly complex and best handled by a computer. (If you're interested, there are several standard textbooks available which describe the *ZAF* and related procedures in detail, for example, Heinrich and Newbury 1991.)

It was soon realized that if a thin electron-transparent specimen was used rather than a bulk specimen, then the correction procedure could be greatly simplified because, to a first approximation, the A and F factors could be ignored and only the Z correction would be necessary. In addition, if thin specimens were used, the analyzed volume would be substantially reduced, giving a much better spatial resolution. (We discuss this latter point in detail in the next chapter.)

These two obvious advantages of thin-foil microanalysis led to the development of the so-called electron microscope microanalyzer (EMMA), pioneered by Duncumb in England in the 1960s. Unfortunately the EMMA was ahead of its time, mainly because the WDS was the only X-ray detector system available. As we have seen, the WDS is handicapped by its poor collection efficiency, rela-

tively cumbersome size, and slow, serial operation. These factors, particularly the poor efficiency, meant that a large probe size (~0.2 μm) had to be used to generate sufficient X-ray intensity for quantification, and therefore the gain in spatial resolution over the EPMA was not so great. Also, the poor stability of the WDS meant that it was necessary to measure the beam current to make sure that the X-ray intensities from both standard and unknown could be sensibly compared. As a result of all these drawbacks, the EMMA never sold well and the manufacturer (AEI) went out of the EM business.

It is ironic that around this time the commercial developments that would transform TEMs into viable AEMs were all taking place. We've seen that the XEDS detector was developed in the late 1960s, and about the same time the development of commercial TEM/STEM systems was beginning. However, before the demise of the EMMAs, they were to play a critical role in the development of the thin-foil microanalysis procedures that we use today. The EMMA at the University of Manchester, operated by Cliff and Lorimer, was refitted with an XEDS system and they soon realized that the pseudo-parallel collection mode, the greater collection efficiency, and the improved stability of the XEDS removed many of the problems associated with WDS on the EMMA. Cliff and Lorimer (1975) showed that quantification was possible using a simplification of Castaing's original ratio equation, in which there was no need to incorporate intensity data from a standard, but simply ratio the intensities gathered from two elements simultaneously in the XEDS. This finding revolutionized thin-foil microanalysis.

35.2. THE CLIFF–LORIMER RATIO TECHNIQUE

The basis for this technique is to rewrite equation 35.1 for two elements A and B in a binary system.

- We have to measure the above-background characteristic intensities, I_A and I_B, simultaneously. This is trivial with an XEDS and therefore there is no need to measure the intensity from a standard.
- We assume that the specimen is thin enough so that we can ignore any absorption or fluorescence. This assumption is called the *thin-foil criterion.*

The weight percents of each element C_A and C_B can be related to the measured intensities by the so-called Cliff–Lorimer equation

$$\frac{C_A}{C_B} = k_{AB}\frac{I_A}{I_B} \qquad [35.2]$$

The term k_{AB} is often termed the Cliff–Lorimer factor. It is actually *not* a constant, so don't be fooled by the use of "*k*." It varies according to the TEM/XEDS system and the kV, as we will see later. Because we are ignoring the effects of absorption and fluorescence, k_{AB} is related to the atomic-number correction factor (Z) in Castaing's original ratio equation. (We will derive this relationship rigorously in Section 35.4.C.) Now to obtain an absolute value for C_A and C_B we need a second equation, and in a binary system we simply assume that A and B constitute 100% of the specimen, so

$$C_A + C_B = 100\% \qquad [35.3]$$

We can easily extend these equations to ternary and higher-order systems by writing extra equations of the form

$$\frac{C_B}{C_C} = k_{BC}\frac{I_B}{I_C} \qquad [35.4]$$

and

$$C_A + C_B + C_C = 100\% \qquad [35.5]$$

You should also note that the *k* factors for different pairs of elements AB, BC, etc., are related, thus

$$k_{AB} = \frac{k_{AC}}{k_{BC}} \qquad [35.6]$$

It is a convention that we define the units of composition as wt.%.

So long as you are consistent, you could define the composition in terms of atomic %, or weight fraction, or any appropriate units. Of course the value of the *k* factor would change accordingly. Thus the Cliff–Lorimer equation is the basis for quantitative microanalysis on the AEM. Let's see how we use it in practice.

35.3. PRACTICAL STEPS FOR QUANTITATIVE MICROANALYSIS

First of all, you should try to use only the K_α lines for the measured intensity. (The K_β is combined with K_α if it cannot be resolved.) Use of L or M lines is more difficult because of the many overlapping lines in each family, but

may be unavoidable if the K_α lines are too energetic for your Si(Li) detector.

We can break the process down into four accumulation steps:

- Accumulate enough counts in the characteristic peaks, I_A, I_B, etc. As we will see below, for acceptable errors, there should ideally be at least 10^4 counts above background in each peak. While you can't always obtain this number in a reasonable time before specimen drift, damage, or contamination limit your analysis, you should always choose the largest probe size which is consistent with maintaining the desired spatial resolution, so you get most current into your specimen.
- Keep your specimen as close to 0° tilt as possible to minimize spurious effects.
- Orient your specimen so the thin portion of the wedge faces the detector to minimize X-ray absorption (see Section 35.5).
- If the area of the specimen is close to a strong two-beam dynamical-diffraction condition, you should tilt the specimen slightly to kinematical conditions.

Anomalous X-ray generation can occur across bend contours or whenever a diffracted beam is strongly excited. This point is not too critical because we quantify using a ratio technique. If the beam has a large convergence angle, which is usually the case, any diffraction effect is further reduced. We will see in Section 35.8 that under certain conditions there are advantages to be gained from such crystallographic effects.

Having accumulated a spectrum under these conditions, how do you quantify it? All you have to do is measure the peak intensities I_A, I_B, etc., and then determine a value for the k_{AB} factor. To determine the peak intensities you first have to remove the background intensity from the spectrum and then you integrate the peak intensity. In a modern computerized MCA system, both these steps are accomplished by one of several available software routines. There are advantages and disadvantages to each approach, so you should pick the one that is most suited to your problem.

35.3.A. Background Subtraction

We are not very precise in the terminology that we use in the discussion of the X-ray background intensity, so it can be confusing. The "background" refers to the intensity under the characteristic peaks in the spectrum displayed on the MCA screen. Now, as we saw back in Chapter 4, these X-rays are generated by the "bremsstrahlung" or "braking radiation" process as the beam electrons interact with the coulomb field of the nuclei in the specimen. The intensity distribution of these bremsstrahlung X-rays decreases continuously as the X-ray energy increases, reaching zero at the beam energy. Thus the energy distribution can be described as a "continuum," although, as we've seen, the phenomenon of coherent bremsstrahlung disturbs this continuum.

> Now we tend to use these three terms—"background," "bremsstrahlung," and "continuum"—interchangeably, although strictly speaking they have these specific meanings.

Remember also that the generated bremsstrahlung intensity is modified at energies below about 2 keV by absorption within the detector and the specimen, so we are usually dealing with a background in the spectrum that looks something like Figure 35.1. The best approach to background subtraction depends on whether the region of interest in your spectrum is in this low-energy regime, and if the characteristic peaks you want to measure are close together or isolated.

Window methods. In the most simple case of isolated characteristic peaks superimposed on a slowly varying background, you can easily remove the background intensity by drawing a straight line below the peak and defining the background intensity as that present below the line, as shown in Figure 35.2. So you get the computer first to define a "window" in the spectrum spanning the width

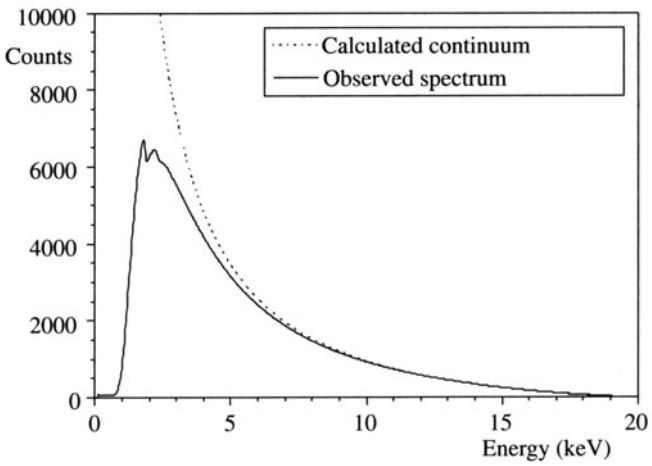

Figure 35.1. The theoretically generated and experimentally observed bremsstrahlung intensity distribution as a function of energy. Both curves are similar until below about 2 keV, when absorption within the specimen and the XEDS system reduces the experimental intensity. Background removal depends on where in the spectrum your characteristic peaks are present.

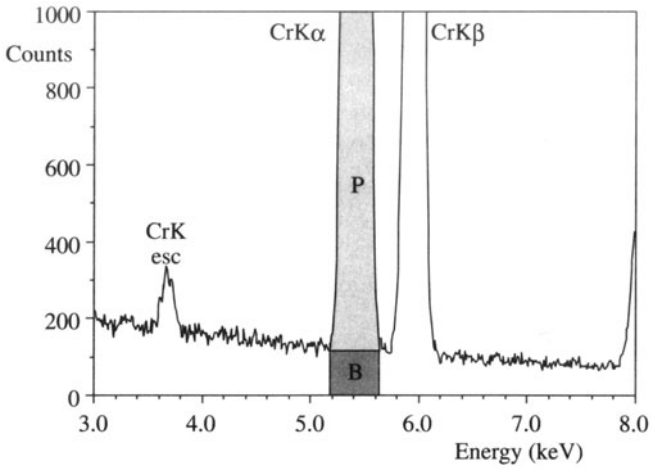

Figure 35.2. The simplest method of estimating the background contribution (B) to the intensity in the characteristic peak (P); a straight line drawn beneath the Cr K_α peak provides a good estimate if the counting statistics are good, and the bremsstrahlung intensity approximates to a slowly varying linear function of energy. There should be no overlap with any other characteristic peaks, and the peaks should be well above ~2 keV.

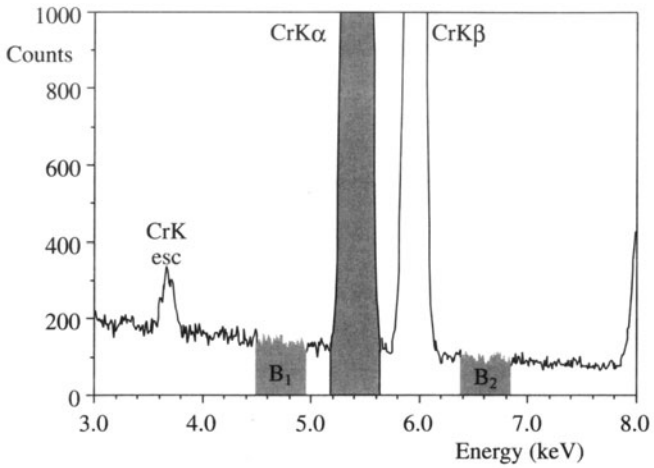

Figure 35.3. Background subtraction can be achieved by averaging the bremsstrahlung intensity in two identical windows (B_1, B_2) either side of the characteristic (Cr K_α and K_β) peaks. There should be no overlap with any other characteristic peaks, and the peaks should be well above ~2 keV.

of the peak, and then draw the line between the background intensities in the channels just outside the window. As with all spectral manipulations, this method gives better results with greater intensity levels in the spectrum. The background intensity variation is then less noisy, so it is easier to decide where the peak ends and the background begins. Furthermore, the background intensity variation better approximates to a straight line.

Another similarly primitive approach involves averaging the bremsstrahlung intensity above and below the characteristic peak by integrating the intensity in two identical windows either side of the peak, as shown in Figure 35.3. You then assume that the average of the two intensities equals the background intensity under the peak, so you subtract this average from the total peak intensity. This assumption is reasonable in the higher-energy regions of the spectrum and when the specimen is thin enough so that the bremsstrahlung is not absorbed in the specimen, which would cause a discrete change in intensity under the peak. When you use this approach it is essential to remember the window width you used, because *identical* windows must be used when subtracting the background both in the unknown spectrum and in the spectrum from the known specimen used to determine the k factor (see Section 35.4).

A typical choice of window width is FWHM, but this throws away a substantial amount of the intensity in the peak. FWTM gives better statistics, but incorporates more bremsstrahlung; 1.2 FWHM is the optimum window.

While the two techniques we just described have the advantage of simplicity, you can't always apply them to real specimens because the spectral peaks may overlap. Also, if the peaks lie in the low-energy region of the spectrum where the background is changing rapidly due to absorption, then neither of these two simple methods gives a good estimate of the background and more sophisticated mathematical approaches are required. We'll now discuss these methods.

Modeling the background. The bremsstrahlung intensity distribution can be mathematically modeled, based on the expression developed by Kramers (1923). The number (N_E) of bremsstrahlung photons of energy E produced in a given time by a given electron beam is given by Kramers' Law:

$$N_E = KZ\frac{(E_0 - E)}{E} \qquad [35.7]$$

Here, Z is the *average* atomic number of the specimen, E_0 is the beam energy in keV, and E is the X-ray energy in keV. The factor K in Kramers' Law actually takes account of numerous parameters. These include

- Kramers' original constant.
- The collection efficiency of the detector.
- The processing efficiency of the detector.
- The absorption of X-rays within the specimen.

All these terms have to be factored into the computer calculation when you use this method of background modeling. In Figure 35.4, the bremsstrahlung is modeled using the Kramers–Small cross section in the DTSA software (see Section 1.5).

Be wary when using this approach because Kramers developed his law for bulk specimens. However, the expression is still used in commercial software and seems to do a reasonable job.

A more satisfactory approach, from a scientific standpoint, is to use the modified Bethe–Heitler formula, as discussed by Chapman *et al.* (1984). This formula is explicitly derived for thin foils and high-keV electrons. This model yields an expression for the bremsstrahlung cross section as a function of the X-ray energy (E) and the atomic number (Z) of the specimen. The slow variation of the cross section with Z leads to the possibility of fitting a simple quadratic expression of the form

$$N_E = \left(\frac{a_0}{E} + a_1 + a_2 E\right)\varepsilon \qquad [35.8]$$

where a_i are simply fitting parameters and ε is the detector efficiency (plotted back in Figure 32.7). The term is only important when modeling the background below ~1.5 keV, and we discuss it in detail later on in Section 35.4.

Modeling the spectrum produces a smooth curve fit that describes the shape of the complete spectrum. This approach is particularly valuable if many characteristic peaks are present, since then it is difficult to make local measurements of the background intensity by a window method. Figure 35.4 shows an example of a spectrum containing three adjacent low-energy peaks, with the background intensity estimated underneath all the peaks.

Filtering out the background. Another mathematical approach to removing the background uses digital filtering. This process makes no attempt to take into account the physics of X-ray production and detection as in Kramers' Law. Rather, it relies on the fact that the characteristic peaks show a rapid variation of intensity as a function of energy (dI/dE is large), while the background exhibits a relatively small dI/dE. This approximation is valid even in the region of the spectrum below ~1.5 keV, where absorption is strong. In the process of digital filtering, the spectrum intensity is "filtered" by convoluting it with another mathematical function. The most common function used is a "top-hat" filter function, so called because of its shape.

When the top-hat filter is convoluted with the shape of a typical X-ray spectrum, it acts to produce a second-difference spectrum, i.e., d^2I/dE^2.

After the top-hat filter, the background with small dI/dE is transformed to a linear function with a value of zero (thus it is "removed"), while the peaks with large dI/dE, although distorted to show negative intensities in some regions, are essentially unchanged as far as the counting statistics are concerned. Figure 35.5A shows schematically the steps required for the filtering process and Figures 35.5B and C show an example of a spectrum before and after digital filtering.

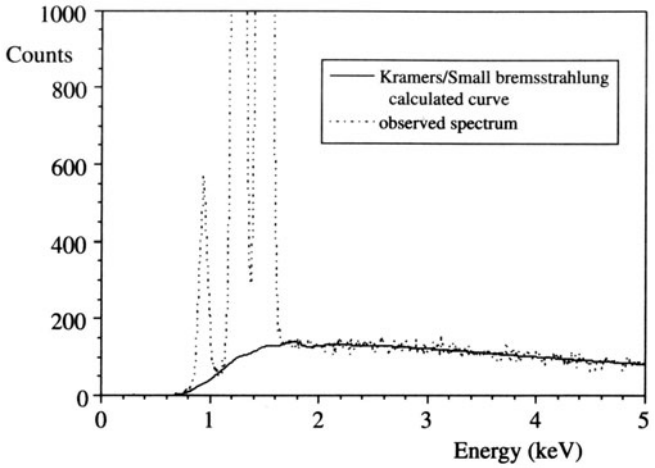

Figure 35.4. The bremsstrahlung intensity modeled using a modified Kramers' Law, which includes the effects of absorption of low-energy X-rays in the specimen and the detector. This method is useful when the spectrum contains overlapping peaks, particularly in the low-energy range, such as the Cu L_α and the Mg and Al K_α lines shown in this spectrum.

In summary, you can remove the background by selecting appropriate windows to estimate the intensity under the peak, or use one of two mathematical modeling approaches. The window method is generally good enough if the peaks are isolated and on a linear portion of the background. The mathematical approaches are most useful for multi-element spectra and/or those containing peaks below ~1.5 keV. You should choose the method that gives you the most reproducible results and you must always take care to apply the same process to both the standard and the unknown. After removing the background, the next thing you have to do is integrate the peak intensities I_A, I_B, etc.

35.3.B. Peak Integration

If you used a window method of background estimation, then the peak intensity is obtained simply by subtracting the estimated background intensity from the total intensity in the chosen window. Therefore, if you drew a line under the peak as in Figure 35.2, then the peak intensity is that above the line.

- If you chose a window of FWHM and averaged the background on either side of the peak, then

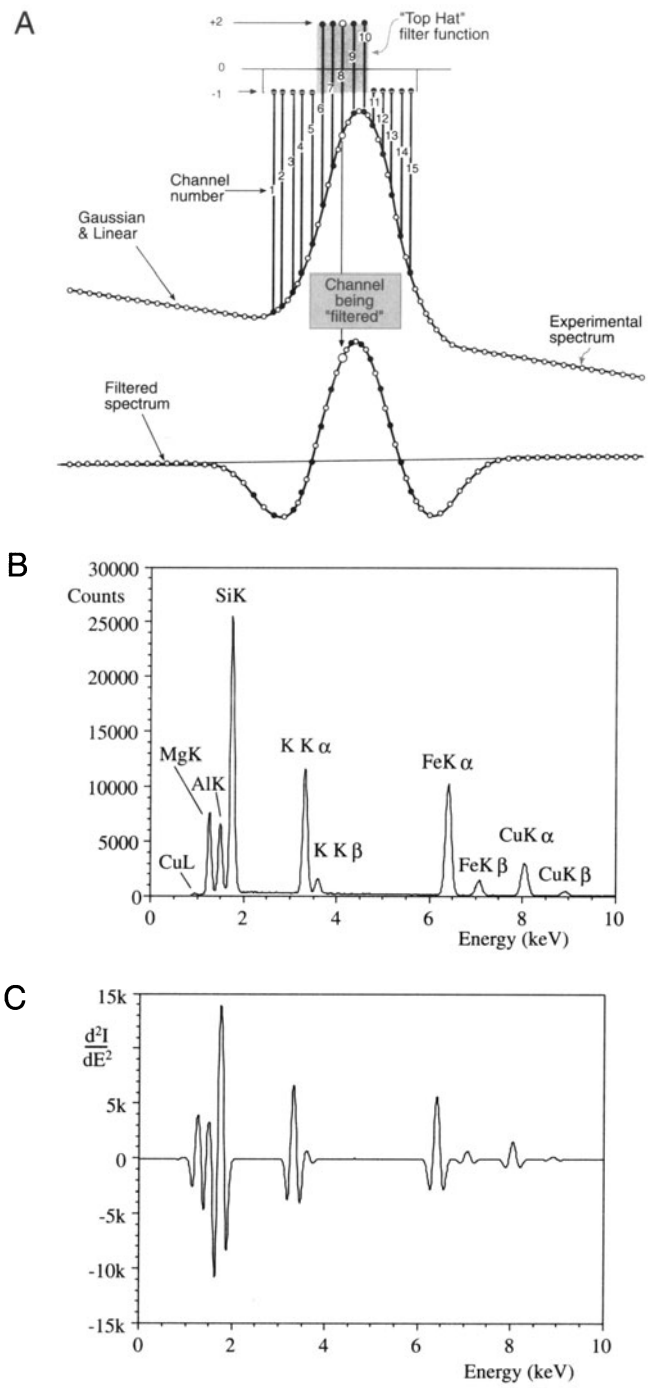

Figure 35.5. (A) Digital filtering involves convolution of a top-hat filter function with the acquired spectrum. To obtain the filtered spectrum, each channel has the top-hat filter applied to it. The channels either side of that being filtered (#8 in this case) are multiplied by the appropriate number in the top-hat function. So channels 1–5 and 11–15 are multiplied by –1 and channels 6–10 by +2. The sum of the multiplications is divided by the total number of channels (15) and allotted to channel #8 in the filtered spectrum at the bottom. The digital filtering process in (A) applied to a spectrum from biotite (B) results in the filtered spectrum (C) in which the background intensity is assigned to zero at all places, and the characteristic peaks remain effectively unchanged.

the average value must be subtracted from the total intensity in the FWHM window.

- If you used a Kramers' Law fit, the usual method of peak integration is to get the computer to fit the peak with a slightly modified Gaussian, and integrate the total counts in the channels under the Gaussian.
- If a digital filter was used, you have to compare the peaks with those that were taken previously from standards, digitally filtered, and stored in a "library" in the computer. The library peaks are matched to the experimental peaks via a multiple least-squares fitting procedure and the intensity determined through calculation of the fitting parameters.

Each of these curve-matching processes is rapid. Each can be used to deconvolute overlapping peaks, and each uses all the counts in the peak. The Kramers' fit and the digital filter have much wider applicability than the simple window methods. However, these computer processes are not invariably the best, nor are they without error.

The Gaussian curve fitting must be flexible enough to take into account several variables:

- The peak width can change as a function of energy or as a function of count rate.
- The peak "tailing" due to incomplete charge collection can vary.
- There may be a low-energy background "shelf" and an absorption edge if the specimen is too thick.

The digital-filter approach requires comparison of experimental peaks with library standards, and this means that you have to create a library of stored spectra under conditions that match those liable to be encountered during microanalysis (particularly, similar count rates and dead times). This is a tedious exercise. However, you do get a figure of merit for the "goodness of fit" between the unknown spectrum and the standard. Usually a chi-squared value is given which has no absolute significance, but is a most useful diagnostic tool. Typically, the chi-squared value should be close to unity for a good fit, although a higher value may merely indicate that some unidentified peaks were not accounted for during the matching process. What you have to watch out for is a sudden increase in chi-squared compared with previous values. This indicates that something has changed from your previous analyses. Perhaps your standard is not giving a good fit to the experimental spectrum and either a new library spectrum needs to be gathered or the experimental peak should be looked at carefully. For example, another small peak may be hid-

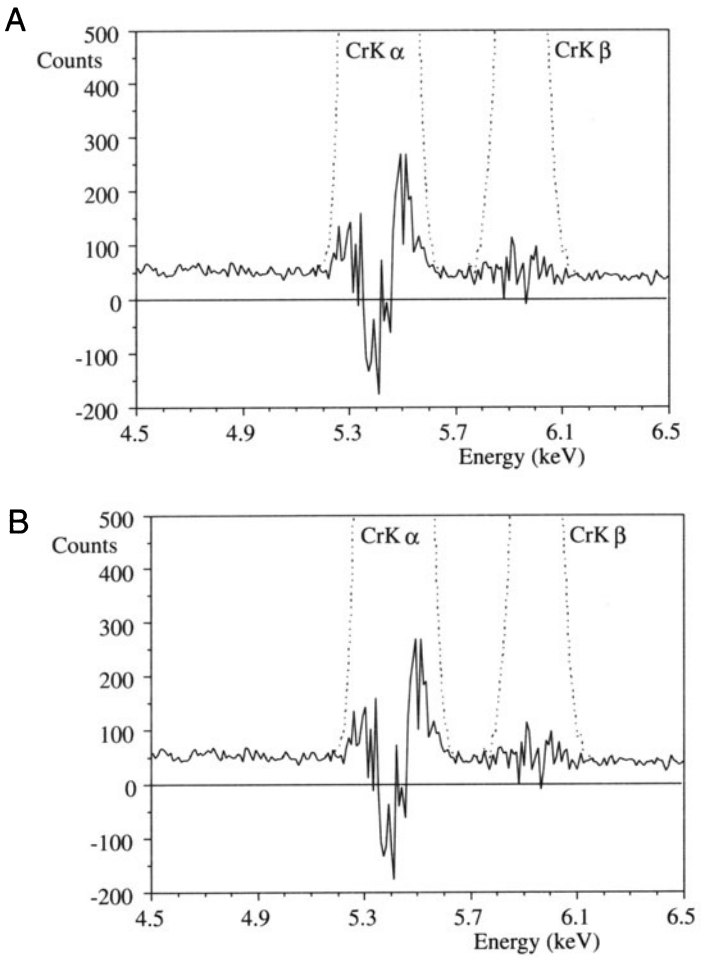

Figure 35.6. (A) A filtered Cr spectrum showing the residual background intensity after the peaks have been removed for integration. The approximately linear residual intensity distribution indicates that the peak matched well with the library standard stored in the computer. (B) A similar filtered spectrum showing the distorted residual counts characteristic of a poor fit with the library standard.

den under the major peak and would need to be deconvoluted from the major peak before integration proceeds. If you suspect a poor fit, you should make the computer display the "residuals," that is, the intensity remaining in the spectrum after the peak has been integrated and removed. As shown in Figure 35.6, you can easily see if a good fit was made (Figure 35.6A) or if the library peak and the experimental peak do not match well (Figure 35.6B).

The point we are making is that any of the above methods is valid for obtaining values of the peak intensity. They should all result in the same answer when used to quantify an unknown spectrum, so long as you apply the same method consistently to both the standard and the unknown.

The next step is to insert the values of the peak intensities in the Cliff–Lorimer ratio equation and know the correct value of the k factor. So we now need to discuss the various ways to obtain k_{AB}.

35.4. DETERMINING *k* FACTORS

Remember that the k factor is not a constant. It is a sensitivity factor that will vary not only with the X-ray detector, the microscope, and the microanalysis conditions, but also with your choice of background-subtraction and peak-integration methods. So values of k factors can be sensibly compared *only* when they were obtained under identical conditions. We will return to this point at the end of this section when we look at various sets of k factors published in the literature. There are two ways you can determine k factors:

- Experimental determination using standards.
- Calculation from first principles.

The first method is slow and laborious but gives the most accurate values. The second method is quick and painless but the results are less reliable.

35.4.A. Experimental Determination of k_{AB}

If you have a thin specimen of known composition, C_A, C_B, etc., then all you have to do, in principle, is place that specimen in the microscope, generate a spectrum, obtain values of I_A, I_B, etc., and insert those values in the Cliff–Lorimer equation (equation 35.2). Since you know C_A and C_B, the only unknown is k_{AB}. However, there are several precautions that you must take before this procedure can be used:

- The standard must be a well-characterized specimen, and it is usually best if it is *single phase*.
- The standard must be capable of being thinned to electron transparency. Ideally, when the specimen is thin there should be no significant absorption or fluorescence of the X-rays from the elements A, B, etc. that you wish to analyze.
- You must be sure that the thinning process did not induce any chemical changes (this is discussed in some detail in Chapter 10).
- It must be possible to select thin regions that are characteristic of the bulk.
- You must be sure that the thin foil is stable under the electron beam at the voltage you intend to use for microanalysis.

This last point may often be the limiting factor in your choice of standards because, as we saw in Section 4.6, you have to take care to avoid not only direct knock-on damage, but also sputtering effects which occur at voltages substantially below the threshold for direct atom displacement. Obviously, both these problems become greater as the beam voltage increases.

The National Institute of Standards and Technology (NIST) has issued a thin standard containing the elements Mg, Si, Ca, Fe, and O (SRM #2063). Unfortunately, X-rays from the lighter elements in this standard film are absorbed significantly in the film, and also in the detector, and so a correction to the measured k factor is necessary. In fact, there are no generally accepted standards that meet all the above criteria for ideal k-factor determination. It is best to use your own judgment in this respect, and also make use of the knowledge gained in previous k-factor studies. The original work of Cliff and Lorimer (1975) was based on crushed mineral standards. Their approach has two advantages:

- Crushing does not affect the chemistry; the stoichiometry is well known.
- Minerals contain Si, thus permitting the creation of a whole series of k_{ASi} factors.

The drawbacks are that the mineral samples often contain more than one phase, or may be naturally nonstoichiometric. Clearly, some prior knowledge of the mineralogy of the sample is essential in order to be able to select the right spectrum to use as a standard. Also, Si K_α X-rays at ~1.74 keV are liable to be absorbed in the XEDS detector, so there may be a systematic difference in k factors determined with different detectors. Finally, silicate minerals often exhibit radiolysis, i.e., chemical changes due to beam-induced breaking of bonds.

Several alternative approaches that attempt to avoid the problems with k_{ASi} have been proposed:

- Wood *et al.* (1984) generated a series of k_{AFe} factors to overcome the Si absorption and the beam sensitivity problems.
- Graham and Steeds (1984) used crystallized microdroplets.
- Sheridan (1989) demonstrated the value of the NIST multi-element glasses.

In all cases the bulk chemistry has to be determined by some acceptable technique, such as EPMA, atomic absorption spectroscopy, or wet chemistry. Since all these techniques analyze relatively large volumes of material, it is best that the standard be single phase. However, because none of these techniques can determine if the specimen is homogeneous on a submicron scale, the only way to find out the level of homogeneity is to carry out many analyses within the AEM to confirm that any variation in your answer is within the expected X-ray statistical fluctuations. A typical k-factor determination therefore involves taking many spectra from different parts of the thin-foil standard to check both the homogeneity and the stability of the specimen. Each spectrum should contain sufficient counts in the peaks of interest to ensure that the errors in the k-factor determination are at least less than $\pm 5\%$ relative and, if possible, less than $\pm$ 3%. So, now we need to consider the errors associated with the X-ray spectra.

35.4.B. Errors in Quantification; the Statistics

An unfortunate aspect of the simple Cliff–Lorimer ratio equation is that it has relatively large errors associated with it. The thin foil that removes the problems of absorption and fluorescence usually results in relatively few X-ray photons per incident electron, compared with bulk specimens. This effect is compounded by the small collection angle of the XEDS detector. The end result is that poor counting statistics are the primary source of error in the quantification. The best way you can limit these errors is to use higher-brightness sources, large electron probes, and thicker specimens, unless absorption is a problem, or spatial resolution is paramount. In any case you should be prepared to count for a long time, assuming that specimen drift and/or contamination don't compromise the data.

> Experimental results show that the X-ray counts in the spectrum obey Gaussian statistics. Hence we can apply simple statistics to deduce the accuracy of any quantification.

The rest of this section is purely statistics. If you know it, then jump ahead.

Given that our characteristic peak is Gaussian, then the standard deviation σ is obtained from

$$\sigma = N^{\frac{1}{2}} \qquad [35.9]$$

where N is the number of counts in the peak above the background. For a single measurement there is a 67% chance that the value of N will be within 1σ of the true value of N. This chance increases to 95% for 2σ and 99.7% for 3σ. If we use the most stringent condition, then the relative error in any single measurement is

$$\text{Relative Error} = \frac{3N^{\frac{1}{2}}}{N}\,100\% \qquad [35.10]$$

Clearly the error decreases as N increases, and hence the emphasis throughout this chapter is on the need to maximize the X-ray counts gathered in your spectra. Since the Cliff–Lorimer equation uses an intensity ratio, we can get a quick estimate of the error by summing the errors in I_A, I_B, and k_{AB} to give the total error in the composition ratio C_A/C_B.

Summing the errors in fact gives an overestimate of the error and, strictly speaking, we should add the relative standard deviations in quadrature using the expression

$$\left(\frac{\sigma_C}{C_A/C_B}\right)^2 = \left(\frac{\sigma_{k_{AB}}}{k_{AB}}\right)^2 + \left(\frac{\sigma_{I_A}}{I_A}\right)^2 + \left(\frac{\sigma_{I_B}}{I_B}\right)^2 \qquad [35.11]$$

So we can determine the error for each datum point in this manner. If we are determining the composition of a single phase, for example during the determination of a k factor, then we can reduce the error by combining the results from n different measurements of the intensity ratio I_A/I_B. The total absolute error in I_A/I_B at a given confidence limit is obtained using the student "t" distribution. For example, in this approach the error is given by

$$\text{Absolute Error} = \frac{(t_{95})^{n-1} S}{n^{\frac{1}{2}}} \qquad [35.12]$$

where $t_{95}{}^{n-1}$ is the student "t" value at the 95% confidence limit for n measurements of k_{AB} (see any statistics text for a list of student "t" values, e.g., Owen 1962). Obviously, you could choose a lower or higher confidence level. Here, S is the standard deviation for n measurements of the intensity, N_i, which on average contain $\bar{N}_i$ counts.

$$S = \left(\sum_{i=1}^{n} \frac{(N_i - \bar{N}_i)^2}{n-1}\right)^{1/2} \qquad [35.13]$$

Hence by increasing the number of measurements n, you can reduce the absolute error in k_{AB}. With enough measurements and a good homogeneous specimen you can reduce the errors in the value of k_{AB} to ±1%, as we will see in the example below. However, remember that this figure must be added to the errors in I_A and I_B. From equation 35.9 it is easy to determine that if we accumulate 10,000 counts in the peak for element A, then the error at the 99% confidence limit is [3 (10,000)$^{1/2}$ / 10,000] × 100%, which is ~3%. A similar value for I_B gives a total error in C_A/C_B of ~±4.5%, using equation 35.11. If you take the time to accumulate 100,000 counts for I_A and I_B, the total error is reduced to ~±1.7%, which represents about the best accuracy that can be expected for quantitative analysis in the AEM. It is appropriate here to go through an illustration of a k_{AB} determination using actual experimental data.

Before deciding that a particular specimen is suitable, it should be checked for its level of homogeneity, and there is a well-established criterion for this. If we take the average value N of many composition determinations, and all the data points fall within ±3$(N)^{1/2}$ of N, then the sample is homogeneous. In other words, this is our *definition of homogeneous*. There are more rigorous definitions, but the general level of accuracy in thin-foil microanalysis is such that there is no need to be concerned about them.

Example

A homogenized thin foil of Cu-Mn solid solution was used to determine k_{CuMn}. The sample was first analyzed by EPMA and found to be 96.64 wt.% Cu and 3.36 wt.% Mn. Since our accuracy is increased by collecting many spectra, a total of 30 were accumulated (n = 30 in equation 35.13). In a typical spectrum, the Cu K_α peak contained 271,500 counts above background and the Mn K_α peak contained 10,800 counts. So if we insert these data into the Cliff–Lorimer equation we get

$$\frac{96.64}{3.36} = k_{CuMn}\frac{271{,}500}{10{,}800}$$

$$k_{CuMn} = 1.14$$

To determine an error on this value of the k factor, equation 35.12 must be used. The student "t" analysis of the k factors from the other 29 spectra gives an error of ±0.01 for a 95% confidence limit. This error of about ±1% relative is about the best that can be achieved using the experimental approach to k-factor determination.

Tables 35.1 and 35.2 summarize many of the available k-factor data in the published literature. You should go and read the original papers, particularly if you want to find out what standards and what conditions were used in their determination.

35.4.C. Calculating k_{AB}

While it is clear that many of the values in the tables are very similar, the differences cannot be accounted for by X-ray statistics alone. Some of the differences arise due to the choice of standard and the reproducibility of the standard. Other differences arise because the data were obtained under different conditions, such as different peak-integration routines. Therefore, the point made at the beginning of this section is worth repeating.

The *k* factors are *not* standards, but sensitivity factors.

Table 35.1. Experimentally Determined k_{ASi} and k_{AFe} Factors for K_α X-ray Lines[a]

Element (A)	k_{ASi} (1) 100 kV	k_{ASi} (2) 100 kV	k_{ASi} (3) 120 kV	k_{ASi} (4) 80 kV	k_{ASi} (5) 100 kV	k_{ASi} (5) 200 kV	k_{AFe} (6) 120 kV	k_{ASi} (7) 200 kV
Na	5.77	3.2	3.57 ± 0.21	2.8 ± 0.1	2.17	2.42		3.97 ± 2.32
Mg	2.07 ± 0.1	1.6	1.49 ± 0.007	1.7 ± 0.1	1.44	1.43	1.02 ± 0.03	1.81 ± 0.18
Al	1.42 ± 0.1	1.2	1.12 ± 0.03	1.15 ± 0.05			0.86 ± 0.04	1.25 ± 0.16
Si	1.0	1.0	1.0	1.0	1.0	1.0	0.76 ± 0.004	1.00
P			0.99 ± 0.016				0.77 ± 0.005	1.04 ± 0.12
S			1.08 ± 0.05		1.008	0.989	0.83 ± 0.03	1.06 ± 0.12
Cl					0.994	0.964		1.06 ± 0.30
K		1.03	1.12 ± 0.27	1.14 ± 0.1			0.86 ± 0.014	1.21 ± 0.20
Ca	1.0 ± 0.07	1.06	1.15 ± 0.02	1.13 ± 0.07			0.88 ± 0.005	1.05 ± 0.10
Ti	1.08 ± 0.07	1.12	1.12 ± 0.046				0.86 ± 0.02	1.14 ± 0.08
V	1.13 ± 0.07			1.3 ± 0.15				1.16 ± 0.16
Cr	1.17 ± 0.07	1.18	1.46 ± 0.03				0.90 ± 0.006	
Mn	1.22 ± 0.07	1.24	1.34 ± 0.04				1.04 ± 0.025	1.24 ± 0.18
Fe	1.27 ± 0.07	1.30	1.30 ± 0.03	1.48 ± 0.1			1.0	1.35 ± 0.16
Co							0.98 ± 0.06	1.41 ± 0.20
Ni	1.47 ± 0.07	1.48	1.67 ± 0.06				1.07 ± 0.006	
Cu	1.58 ± 0.07	1.60	1.59 ± 0.05		1.72	1.50	1.17 ± 0.03	1.51 ± 0.40
Zn	1.68 ± 0.07				1.74	1.55	1.19 ± 0.04	1.63 ± 0.28
Ge	1.92							1.91 ± 0.54
Zr								3.62 ± 0.56
Nb							2.14 ± 0.06	
Mo	4.3		4.95 ± 0.17				3.8 ± 0.09	
Ag	8.49		12.4 ± 0.63				9.52 ± 0.07	6.26 ± 1.50
Cd	10.6				9.47	6.2		
In								7.99 ± 1.80
Sn	10.6							8.98 ± 1.48
Ba					29.3	17.6		21.6 ± 2.6

Table 35.2. Experimentally Determined k_{ASi} and k_{AFe} Factors for L_α X-ray Lines[a]

Element (A)	k_{ASi} (8) 100 kV	k_{ASi} (5) 100 kV	k_{ASi} (5) 200 kV	k_{ASi} (9) 100 kV	k_{AFe} (6) 120 kV	k_{ASi} (7) 200 kV
Cu		8.76	12.2			
Zn		6.53	6.5			8.09 ± 0.80
Ge						4.22 ± 1.48
As						3.60 ± 0.72
Se						3.47 ± 1.11
Sr					1.21 ± 0.06	
Zr					1.35 ± 0.1	2.85 ± 0.40
Nb					0.9 ± 0.06	
Mo				2.0		
Ag	2.32 ± 0.2				1.18 ± 0.06	2.80 ± 1.19
In					2.21 ± 0.07	2.86 ± 0.71
Cd		2.92	2.75			
Sn	3.07 ± 0.2					
Ba		3.38	2.94			3.36 ± 0.58
Ce				1.4		
Sn	3.1 ± 0.2			1.3		
W	3.11 ± 0.2			1.8		3.97 ± 1.12
Au	4.19 ± 0.2	4.64	3.93		3.1 ± 0.09	4.93 ± 2.03
Pb	5.3 ± 0.2	4.85	4.24	2.8		5.14 ± 0.89

[a]Sources: (1) Cliff and Lorimer (1975), (2) Wood *et al.* (1981), (3) Lorimer *et al.* (1977), (4) McGill and Hubbard (1981), (5) Schreiber and Wims (1981), (6) Wood *et al.* (1984), (7) Sheridan (1989), (8) Goldstein *et al.* (1977), (9) Sprys and Short (1976).

The only conditions under which you can expect the k factors obtained on different AEMs to be identical are if you use the *same* standard at the *same* accelerating voltage, *same* detector configuration, and *same* peak-integration and background-subtraction routines. Even then there will be differences if one or more of the measured X-ray lines is not gathered by the detector with 100% efficiency; the X-ray may be either absorbed by the detector or it may be too energetic and pass straight through the detector.

You may not be able to obtain a suitable standard. For example, you might be working in a system in which no stoichiometric phases exist or accuracy might not be critical, but you need a quick analysis. Then you can calculate an approximate k factor. The programs necessary to calculate k_{AB} are stored in the computer and will give a value of k in a fraction of a second. The calculated value should be accurate to within ±20% relative. Often, this level of accuracy is all you need to draw a sensible conclusion concerning the problem.

Calculating k factors is the recommended approach when a quick answer is required and accuracy is not essential.

We will derive the expression for calculating the k factor from first principles, starting in a manner similar to the development of the expressions for the analysis of bulk samples in the EPMA. The derivation gives a good illustration of the relationship between bulk and thin-film microanalysis, and provides insight into the details of X-ray interactions with solids. In addition, the equations will provide us with the necessary grounding to pursue the problems of absorption and fluorescence in thin foils, when they occur. A full discussion of this derivation is given in the paper by Williams and Goldstein (1991). If you don't need to know the details of this derivation, you may wish to move on to the final expression given in equation 35.23.

The intensity of the *generated* X-ray emission from element A in the specimen, I_A^{Spec*}, is

$$I_A^{Spec*} = \Phi_A^{\Delta\rho t} \int_0^{\infty} \varphi(\rho t)\, e^{-\chi\rho t} \left(1 + \delta_A\right) d(\rho t) \qquad [35.14]$$

- The term $\Phi_A^{\Delta\rho t}$ is the X-ray emission (in cps) generated from element A in an isolated thin film of the specimen with mass thickness $\Delta\rho t$; the thickness of this isolated film is Δ and its mass thickness is ρt (it is *not* the change in ρt).
- The term $\varphi(\rho t)$ is the depth distribution of X-ray production. We define it as the ratio of the X-ray emission from a layer of element A of thickness $\Delta\rho t$ at a depth t in the specimen to the X-ray emission from an identical, but isolated, film.
- The expression $e^{-\chi\rho t}$ accounts for X-ray absorption in the specimen, where χ is defined as

$$\chi = \left.\frac{\mu}{\rho}\right]_{Spec}^{A} \operatorname{cosec}\alpha \qquad [35.15]$$

- The term $\mu/\rho]_{Spec}^{A}$ is the mass absorption coefficient for X-rays from element A in the specimen and α is the X-ray take-off angle.

X-rays from element A may also be fluoresced by other characteristic X-rays emerging from the specimen. The fluorescence contribution to the generated intensity is $(1+\delta_A)$. We can write an expression for the intensity of X-rays from an isolated thin film within a specimen as

$$\Phi_A^{\Delta\rho t} = N\left(\frac{Q\omega a}{A}\right)_A C_A \Delta\rho t \qquad [35.16]$$

where N is Avogadro's number. The subscript A denotes the element A in each case, Q_A is the ionization cross section, ω_A is the fluorescence yield for the characteristic X-rays, A_A is the atomic weight and C_A is the weight fraction of the element.

The use of the weight fraction rather than the atomic fraction is an anomaly which has persisted from the earliest days of microanalysis, when it was thought by Castaing that an atomic number correction was not required.

The remaining term "a" is the relative transition probability. This term takes account of the fact that when a K-shell electron is ionized, the atom will return to ground state through the emission of either a K_α or K_β X-ray. The term "a" in equation 35.14 in this case would be given by

$$a = \frac{I(K_\alpha)}{I\left(K_\alpha + K_\beta\right)} \qquad [35.17]$$

You may remember that we listed the relative "weights" of the X-ray lines in Table 4.1. We can easily apply equation 35.14 to thin-film specimens. For such specimens we can then make some simplifications:

- Assume that the electrons only lose a small fraction of their energy in traversing the specimen. Therefore, Q_A is taken as a constant, and evaluated for the incident beam energy E_0.

- Limit the integral in equation 35.12 to the foil thickness t.

Thus if we substitute equation 35.16 into equation 35.14, we find

$$I_A^{Spec} = N\left(\frac{Q\omega a}{A}\right)_A C_A \Delta\rho t \int_0^t \varphi_A(\rho t)\, e^{-\chi\rho t}(1+\delta_A)\, d(\rho t) \quad [35.18]$$

The Cliff–Lorimer equation assumes that we can measure two characteristic X-ray intensities simultaneously and so we can ratio two equations like equation 35.18, cancel N and $\Delta(\rho t)$, and rewrite them thus

$$\frac{I_A^{Spec*}}{I_B^{Spec*}} = \frac{C_A \frac{Q_A \omega_A a_A}{A_A} \int_0^t \varphi_A(\rho t)\, e^{-\chi\rho t}(1+\delta_A)\, d(\rho t)}{C_B \frac{Q_B \omega_B a_B}{A_B} \int_0^t \varphi_B(\rho t)\, e^{-\chi\rho t}(1+\delta_B)\, d(\rho t)} \quad [35.19]$$

This equation can be conveniently shortened to

$$\frac{I_A}{I_B} = \frac{C_A}{C_B}(ZAF) \quad [35.20]$$

where Z, A, and F stand for the atomic-number, absorption, and fluorescence corrections, respectively. Now remember that the Cliff–Lorimer equation (equation 35.2) assumes that A and F are negligible in a thin foil. We therefore rearrange equation 35.20 to look like equation 35.2

$$\frac{C_A}{C_B} = \frac{1}{Z}\frac{I_A}{I_B} \quad [35.21]$$

By comparison of the two equations (35.2 and 35.19) we can write an expression for k_{AB}

$$k_{AB} = \frac{1}{Z} = \frac{(Q\omega a)_B A_A}{(Q\omega a)_A A_B} \quad [35.22]$$

Thus, as we mentioned at the start of the discussion on quantification, the Cliff–Lorimer k factor for thin-foil analysis is related to the atomic-number correction factor (Z) for bulk specimen microanalysis. From equation 35.22 we can easily see which experimental factors determine the value of k.

- Obviously, the accelerating voltage is a variable since Q is strongly affected by the kV.
- The atomic number affects ω, A, and a.
- The choice of peak-integration method will also affect a.

Therefore, in order to calculate and compare different k factors, it is imperative to define these conditions very clearly, as we have taken pains to emphasize.

Equation 35.20 assumes that equal fractions of the X-rays generated by elements A and B are collected and processed by the detector. This assumption will only be true if the same detector is used and the X-rays are neither strongly absorbed nor pass completely through the detector. However, as we have already seen in Chapter 32, X-rays below ~1.5 keV are absorbed significantly by the Be window and X-rays above ~20 keV pass through a 3-mm Si detector with ease. Under these circumstances it is necessary to modify the k-factor expression, equation 35.22, in the following manner

$$k_{AB} = \frac{1}{Z} = \frac{(Q\omega a)_A}{(Q\omega a)_B}\frac{A_B}{A_A}\frac{\varepsilon_A}{\varepsilon_B} \quad [35.23]$$

The symbol ε represents simply a detector-efficiency term (plotted back in Figure 32.7) that we can write as follows

$$\varepsilon_A = \exp\left(-\left[\frac{\mu}{\rho}\right]_{Be}^{A} \rho_{Be} t_{Be}\right) \exp\left(-\left[\frac{\mu}{\rho}\right]_{Au}^{A} \rho_{Au} t_{Au}\right) \cdot \exp\left(-\left[\frac{\mu}{\rho}\right]_{Si}^{A} \rho_{Si} t_{Si}\right)\left\{1 - \exp\left(-\left[\frac{\mu}{\rho}\right]_{Si}^{A} \rho_{Si} t'_{Si}\right)\right\} \quad [35.24]$$

Here, the mass absorption coefficient for the X-rays from element A are required for the Be window, the Au (or other) contact layer, the Si dead layer, and the Si intrinsic region (thickness t'). We can also write a similar expression for an IG detector. These various detector parameters each have density ρ (available from standard elemental density tables) and thickness t. Typical values of t for each part of the detector were discussed in Chapter 32. The first three terms thus account for absorption of weak X-rays passing through the Be window, the Au contact layer, and the Si dead layer before entering the detector. The last term adjusts the k factor for X-rays that *do not* deposit their energy in the active region of the detector which has density ρ and thickness t'.

While equations 35.23 and 35.24 look simple for a computer to solve, the values that have to be inserted in the equations for the various terms are not always well known, or cannot be measured accurately. For example, we do not know the best value of Q for many elements in the range of voltages typically used in the AEM (100–400 kV). There are considerable differences of opinion in the literature concerning the best way to choose a value for Q. The two major approaches used are:

- Assume various empirical parameterization processes (e.g., Powell 1976).
- Interpolate values of Q to give the best fit to experimental k factors (Williams *et al.* 1984).

Table 35.3a. Calculated k_{AFe} Factors for K Lines Using Different Theoretical Cross Sections[a]

Element A	k_{MM}	k_{GC}	k_{P}	k_{BP}	k_{SW}	k_{Z}
Na	1.42	1.34	1.26	1.45	1.17	1.09
Mg	1.043	0.954	0.898	1.03	0.836	0.793
Al	0.893	0.882	0.777	0.877	0.723	0.696
Si	0.781	0.723	0.687	0.769	0.638	0.623
P	0.813	0.759	0.723	0.803	0.671	0.663
S	0.827	0.776	0.743	0.817	0.688	0.689
K	0.814	0.779	0.755	0.807	0.701	0.722
Ca	0.804	0.774	0.753	0.788	0.702	0.727
Ti	0.892	0.869	0.853	0.888	0.807	0.835
Cr	0.938	0.925	0.917	0.936	0.887	0.909
Mn	0.98	0.974	0.970	0.979	0.953	0.965
Fe	1.0	1.0	1.0	1.0	1.0	1.0
Co	1.063	1.069	1.074	1.066	1.096	1.079
Ni	1.071	1.085	1.096	1.074	1.143	1.23
Cu	1.185	1.209	1.227	1.19	1.31	1.24
Zn	1.245	1.278	1.305	1.255	1.44	1.32
Mo	3.13	3.52	3.88	3.27	3.84	3.97
Ag	4.58	5.41	6.23	4.91	5.93	6.28

The other major variable in equation 35.24 is the Be window thickness, which is nominally 7.5 μm but in practice may be substantially thicker. Tables 35.3a and b list calculated k factors obtained using various expressions for Q. As you can see, the value of k may easily vary by >±10%, particularly for the lighter elements and the heavier elements. This variation is due to the uncertainties in the detector-efficiency terms in equation 35.22. The values of k_{AB} for the L lines are even less accurate than for the K lines, mainly because the values of Q for the L lines are somewhat speculative. There are no data available for calculated k factors for M lines. Under these circumstances, experimental determination is the only approach. This point again emphasizes the advantages of K-line analysis where possible. When the heavy elements are being studied, the L or M lines, which may be the strongest in a spectrum from a Si(Li) detector, will undoubtedly give rise to greater errors than the K lines, which may only be detectable with an IG system.

Table 35.3b. Calculated k_{AFe} Factors for L Lines Using Different Theoretical Cross Sections[a]

Element	k_{MM}	k_{P}	k_{HP}	k_{SW}	k_{Z}
Sr[a]	1.73	1.33	1.32	1.64	1.39
Zr[a]	1.62	1.26	1.24	1.51	1.33
Nb[a]	1.54	1.21	1.18	1.43	1.28
Ag[a]	1.43	1.16	1.09	1.26	1.26
Sn	2.55	2.09	1.93	2.21	2.30
Ba	2.97	2.52	2.25	2.49	2.83
W	3.59	3.37	2.68	2.80	3.88
Au	3.94	3.84	2.94	3.05	4.43
Pb	4.34	4.31	3.o5	3.34	4.97

[a]k factors use the L intensity from the L_{α} and L_{β} lines. MM = Mott–Massey; GC = Green–Cosslett; P = Powell; BP = Brown–Powell; SW = Schreiber–Wims; Z = Zaluzec.

The combination of uncertainties in Q and in the detector parameters is the reason why calculated k factors are not very accurate, usually no better than ±10–20% relative. The computer system attached to the AEM will have predetermined values of all the terms in equations 35.21 and 35.22 stored in its memory. You don't usually have control over which particular parameters are being used. However, you should at least ask the manufacturer to list the sources of the values of Q, ω, and a in the computer. You should then carry out a cross-check calculation with a known specimen to ensure that the calculated k factor gives the correct answer.

If you replace or service a detector, which is not an unusual occurrence on an AEM, then the new detector parameters must be inserted into the software.

We cannot recommend a "best" set of values for Q, ω and a, but the values of Q given by Powell (1976), ω by Bambynek *et al.* (1972), and a by Schreiber and Wims (1982) have been used in the past. Also, we can't give you specific detector parameters, so you should obtain an estimate from the manufacturer. The values of μ/ρ which we recommend are those determined by Heinrich (1986), although there is still considerable uncertainty in the mass absorption coefficients for the low-energy X-rays from the light elements. If

you use the DTSA program from NIST (see Section 1.5), you may find that it predicts a worse value.

> Remember that the problem is that all software packages use preset values in their calculations and these may vary from package to package.

Figures 35.7A and B show a comparison of the two methods of *k*-factor determination. The experimental data are shown as individual points with error bars, and the solid lines represent the range of calculated *k* factors, depending on the particular value of *Q* used in equation 35.21. The relatively large errors possible in the calculated *k* factors are clearly seen, and comparison of the K-line data in Figure 35.7A with the L-line data in Figure 35.7B again emphasizes the advantages of using K lines for the analysis where possible. Similar data for M lines are almost nonexistent, but data for the K lines from the heavier elements will become more common if IG detectors are more widely used.

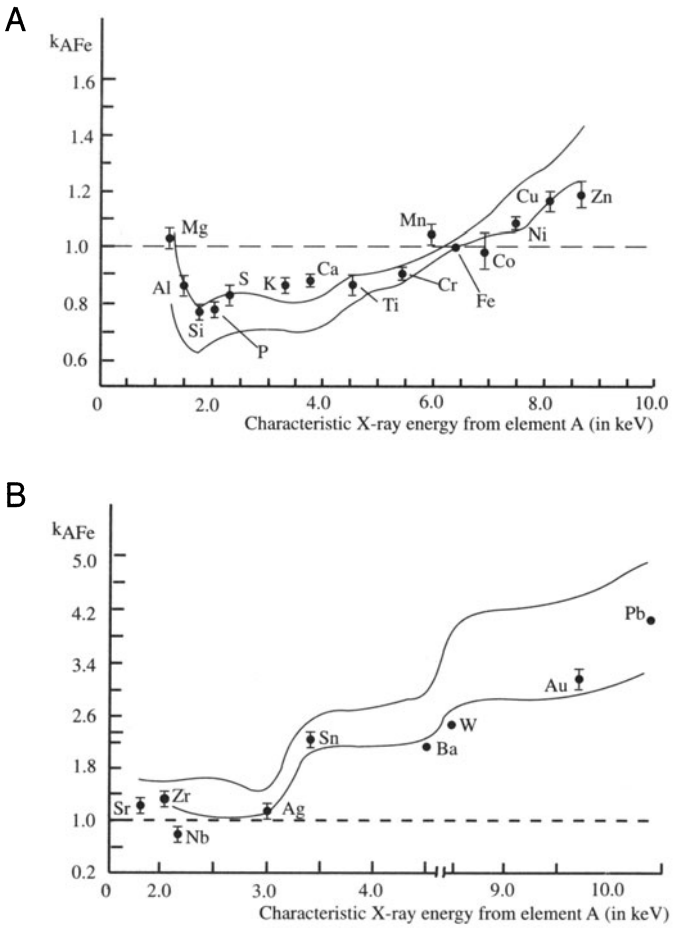

Figure 35.7. (A) Experimental k_{AFe} factors for the K_α X-rays from a range of elements A with respect to Fe. The solid lines represent the spread of calculated *k* factors using different values for the ionization cross section. (B) Similar data for L_α lines from relatively high-*Z* elements. The errors in the calculated values of *k* are large, reflecting the uncertainties in L-line ionization cross sections.

We can summarize the *k*-factor approach to microanalysis in the following way:

- The Cliff–Lorimer equation has the virtue of simplicity. All you have to do is specify all the variables and treat the standard and unknown in an identical manner.
- You are better off calculating k_{AB} if you prefer speed to accuracy. Experimental determination is best if you wish to have a known level of confidence in the numbers that you produce.

The point at which the simple Cliff–Lorimer approach breaks down is when the thin-foil criterion is invalid. Absorption is far more common than fluorescence in thin foils. You must be wary of absorption when you have X-ray lines in your spectrum that differ in energy by >5–10 keV, particularly if any are light-element X-rays. To understand why this is so, we must investigate the absorption correction factor.

35.5. ABSORPTION CORRECTION

Preferential absorption of the X-rays from one of the elements in your specimen means that the detected X-ray intensity will be less than the generated intensity and so C_A is no longer simply proportional to I_A. So you have to modify your *k* factor to take into account the reduction in I_A. This is a problem if your specimen is too thick, or if one or more of the characteristic X-rays has an energy less than ~1 keV (i.e., light element analysis). If we define k_{AB} as the true sensitivity factor when the specimen thickness $t = 0$, then the effective sensitivity factor for a specimen in which absorption occurs is given by k_{AB}^* where

$$k_{AB}^* = k_{AB}(ACF) \qquad [35.25]$$

The absorption correction factor (ACF) is the *A* term in equation 35.20 and this can be written out fully, incorporating the expression for χ from equation 35.15, to give

$$\mathrm{ACF} = \frac{\displaystyle\int_0^{*t} \left\{ \varphi_B(\rho t)\, e^{-\left(\frac{\mu}{\rho}\right]_{Spec}^{B} \rho t \,\mathrm{cosec}\,\alpha} \right\} d(\rho t)}{\displaystyle\int_0^{t} \left\{ \varphi_A(\rho t)\, e^{-\left(\frac{\mu}{\rho}\right]_{Spec}^{A} \rho t \,\mathrm{cosec}\,\alpha} \right\} d(\rho t)} \qquad [35.26]$$

In this expression $\mu/\rho]^A_{Spec}$ is the mass absorption coefficient of X-rays from element *A* in the specimen, α is the detector take-off angle, ρ is the density of the specimen, and *t* is the thickness. Since the units of μ/ρ are usually cm^2/gm, be sure to use ρ in gm/cm^3 and t in cm, rather than SI units. Obviously, the value of the ACF is unity when no absorption occurs. Typically, if the ACF is >10% then the absorption is significant, since 10% accuracy is routinely attainable in quantitative microanalysis using experimental *k* factors. However, accuracy better than 10% can be obtained if you decide what constitutes a "significant" level of absorption for the problem at hand and the accuracy required of the data. Let's now look at each of the terms and the problems associated with determining their value.

Again, we recommend that you use the values of μ/ρ given by Heinrich (1986). The value of μ/ρ for a particular X-ray (e.g., from element A) within the specimen is the sum of the mass absorption coefficients for each element times the weight fraction of that element, so

$$\left.\frac{\mu}{\rho}\right]^A_{Spec} = \sum_i \left(\left.\frac{C_i\mu}{\rho}\right]^A_i \right) \qquad [35.27]$$

where C_i is the fractional concentration of element *i* in the specimen such that

$$\sum_i C_i = 1 \qquad [35.28]$$

The absorption of X-rays from element *A* by all elements *i* in the specimen is summed, including self absorption by element *A* itself, absorption by elements that may not be of interest in the experiment, and even by materials whose X-rays might not be detectable.

An example of this phenomenon occurs when Mg is being quantified in homogeneous NiO-MgO. The Mg K_α X-rays will be absorbed by oxygen, even if the O K_α X-ray is not of interest or cannot be detected because a Be window detector is being used. This effect is shown in Figure 35.8, which shows an increase in the intensity ratio (Ni K_α/Mg K_α) as a function of thickness due to the increased absorption of the Mg K_α X-rays. (Absorption appears in an exponential term.) If we correct for the absorption by Ni, the slope of the line is reduced, but only when the effects of absorption by oxygen are taken into account does the slope become zero, as it should be for a homogeneous specimen (Bender *et al.* 1980).

In equation 35.26, the depth distribution of X-ray production $\varphi(\rho t)$ is assumed to be a constant and equal to unity. That is, a uniform distribution of X-rays is generated at all depths throughout the foil. This is a reasonable first approximation in thin foils, but in bulk specimens $\varphi(\rho t)$ is a strong function of *t*. Depending on the thickness of the foil, it is possible that this assumption may be the limiting factor in the accuracy of the absorption correction, but for most thin foils, particularly if *Z* is < 30, variations in $\varphi(\rho t)$ can be ignored. If $\varphi(\rho t)$ does affect the absorption correction, then it will result in a slight overcompensation for the effects of absorption, which will get worse as the thickness increases.

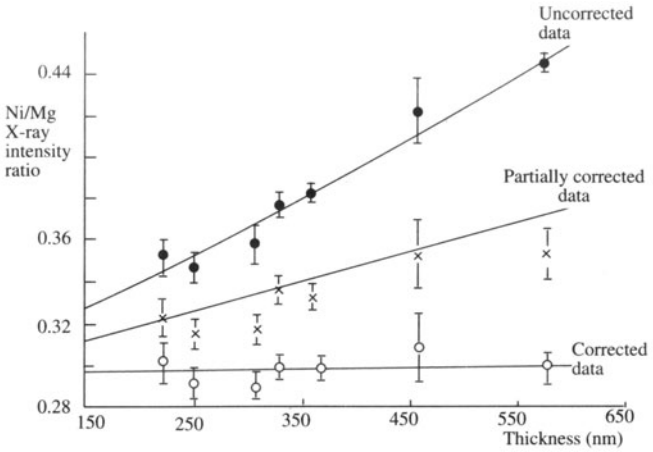

Figure 35.8. The upper curve shows the raw Ni K_α/Mg K_α intensity ratio as a function of thickness in a homogeneous sample of NiO-MgO. The slope indicates strong absorption of Mg K_α X-rays. The middle curve shows the effect of correcting for absorption of the Mg K_α line by Ni and the bottom line shows the effect of a further correction for absorption of the Mg K_α line by O to give the expected horizontal line.

The measurement of $\varphi(\rho t)$ for bulk specimens is a well-established procedure. The few studies in thin specimens show an increase in $\varphi(\rho t)$ with specimen thickness, although the increase is no more than about 5% in foil thicknesses of <300 nm. Therefore, the assumption that $\varphi(\rho t)$ equals unity does indeed appear reasonable. The fact that we use a ratio of the two $\varphi(\rho t)$ terms in the absorption equation also helps to minimize the effects of this assumption.

We assume that $\varphi(\rho t)$ equals unity. Then we can simply use equation 35.26 to give

$$ACF = \left(\frac{\left.\frac{\mu}{\rho}\right]^A_{Spec}}{\left.\frac{\mu}{\rho}\right]^B_{Spec}} \right) \left(\frac{1 - e^{-\left(\left.\frac{\mu}{\rho}\right]^B_{Spec} \rho t \operatorname{cosec} \alpha \right)}}{1 - e^{-\left(\left.\frac{\mu}{\rho}\right]^A_{Spec} \rho t \operatorname{cosec} \alpha \right)}} \right) \qquad [35.29]$$

So we still need to know the values of ρ and *t* for our specimens.

The density of the specimen (ρ) can be estimated if you know the unit-cell dimensions, e.g., from convergent-beam electron diffraction

$$\rho = \frac{n A}{V \mathrm{N}} \qquad [35.30]$$

where n is the number of atoms of average atomic weight A in a unit cell of volume V, and N is Avogadro's number.

The absorption path length (t') is a major variable in the absorption correction. Fortunately, it is also the one over which you, the operator, have the most control. In the simplest case of a parallel-sided thin foil of thickness t at 0° tilt, the absorption path length, as shown in Figure 35.9, is given by

$$t' = t \operatorname{cosec} \alpha \qquad [35.31]$$

where α is the detector take-off angle. To minimize this factor, it is obvious that your specimen should be as thin as possible and the value of α as high as possible. There are many ways to determine the foil thickness which we have discussed at various points in this text; they are summarized in Section 36.6. No method is universally applicable, and few are either easy or accurate. The value of α with the specimen at 0° tilt is fixed by the design geometry of the stage and the only way to vary α is by tilting the specimen. As we have seen, there are good reasons not to tilt the specimen beyond about 10°, because of the increase in spurious X-rays, but if there is a severe absorption problem, then decreasing t' by tilting the specimen toward the detector is a sensible first step toward minimizing the problem.

In some AEMs it is necessary to tilt the specimen toward the detector before any X-rays can be detected. Matters get even more complicated if your detector axis is not orthogonal to the tilt axis. Such a design is very poor from an analytical standpoint but, even under these conditions, the geometry is relatively straightforward and Zaluzec *et al.* (1981) have listed all the necessary equations.

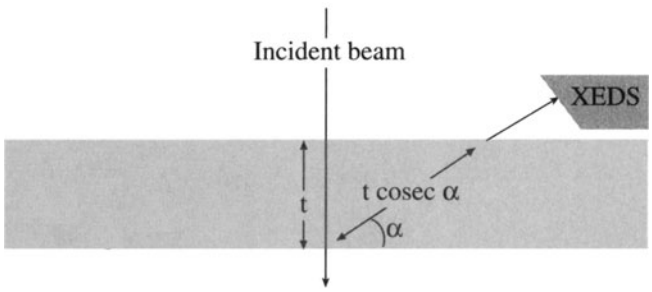

Figure 35.9. Relationship between the specimen thickness t and the absorption path length t cosecα for a take-off angle α.

Fluorescence is usually a minor effect and often occurs for X-rays that are not of interest.

So far we've assumed that the specimen is parallel-sided, but this is uncommon. Most thin-foil preparation methods result in wedge-shaped foils, and under these circumstances the detector must always be "looking" toward the thin edge of the specimen so that the X-ray path length is minimized, as we already mentioned in Figure 33.3. The only way to ascertain if this is a problem is to measure the thickness at each analysis point. Because this is such a tedious exercise, a method has been developed to correct for absorption without measuring t, as we discuss in the next section.

Because the sample density, ρ, and the values of μ/ρ vary with the composition of the specimen (see equations 35.22 and 35.23), the complete absorption correction procedure is an iterative process. The first step is to use the Cliff–Lorimer equation without any absorption correction and thus produce values for C_A and C_B. From these values, you perform a first iteration calculation of μ/ρ and ρ, and generate modified values of C_A and C_B, and so on. Usually, the calculation converges after two or three iterations.

In summary, there is substantial room for error in determining the various terms to insert into the ACF. For example, the ACF for k_{NiAl} in Ni_3Al, which is a strongly absorbing system, varies from ~5.5% to ~12% when the specimen doubles in thickness from 40 nm to 80 nm. This change is still quite small and within the limits of all but the most accurate microanalyses. In FeNi, which is a weakly absorbing system, a similar change in thickness would change the ACF for k_{FeNi} from ~0.6% to ~1.3%, which is negligible.

It should always be remembered that large errors will only occur in strongly absorbing systems and/or very thick specimens.

35.6. EXTRAPOLATION TECHNIQUES FOR ABSORPTION CORRECTION

A different approach to the absorption problem has been developed by Horita *et al.* (1987) and Van Cappellen (1990) which neatly avoids the problems of measuring the thickness at each analysis point, but does require that you measure the beam current. This is the way you should proceed with the absorption correction if it is at all possible.

You still need to know μ/ρ, ρ, and α, but not t. This approach uses a simplified correction factor

$$ACF' \simeq e^{-\left(\left[\frac{\mu}{\rho}\right]^{B}_{Spec} - \left[\frac{\mu}{\rho}\right]^{A}_{Spec} \frac{\rho t}{2} \operatorname{cosec} \alpha\right)} \quad [35.32]$$

which assumes that all X-rays are generated at $t/2$, ignoring $\varphi(\rho t)$ effects, and requires that the X-rays from one of the two elements are not absorbed. Applying the ACF′ to the measured intensity ratios, we can show that, if we measure k_{AB} over a range of thicknesses, we can extrapolate to $(k_{AB})_0$ at $t = 0$ to give

$$\log_{10}(k_{AB}) = \log_{10}(k_{AB})_0 + \frac{\Delta_{AB}}{\varphi} I_x \quad [35.33]$$

where Δ_{AB} is related to the difference in μ/ρ for X-rays from elements A and B:

$$\Delta_{AB} = 0.217\left(\left[\frac{\mu}{\rho}\right]^{A}_{Spec} - \left[\frac{\mu}{\rho}\right]^{B}_{Spec}\right)\rho \operatorname{cosec}(\alpha) \quad [35.34]$$

and

$$\varphi = C_A\left(\frac{Q\,\omega\,a}{A}\right)_A i_A \quad [35.35]$$

for element A, where all the terms are described in equation 35.16, except for the electron probe current i_A, which is assumed constant.

So to apply this method, you need to keep the beam current and X-ray acquisition time constant, and the specimen must contain one X-ray that shows negligible absorption, as shown in Figure 35.10.

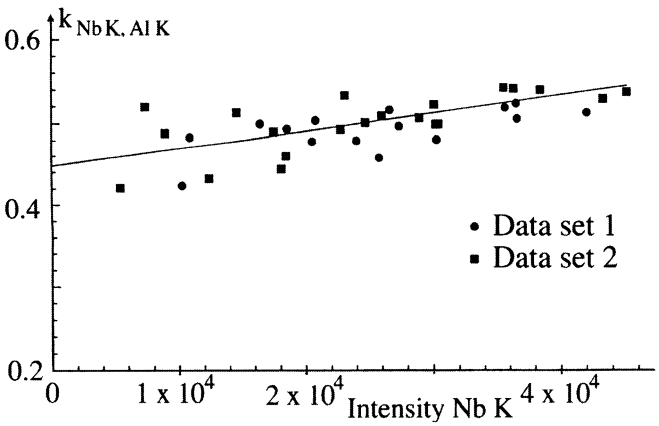

Figure 35.10. A plot of two independent sets of k-factor data for a Nb-Al alloy at 300 kV, showing the variation of the effective k factor with thickness as indicated by the Nb K_α X-ray intensity. The Al K_α X-rays which are absorbed give increasing effective k factors with thickness. X-rays for which absorption is insignificant would give a constant k factor with thickness.

The method can be extended to the microanalysis of unknown specimens by using the extrapolation method to determine the absorption-free intensity ratio at zero thickness, and using this ratio in combination with the k_{AB} factor at zero thickness to give a value of C_A/C_B. This k factor is then applied to the calculation of the composition using the intensity ratio measured at the same thickness.

Obviously, it is very time-consuming to do the full absorption correction as accurately as we would like, because of all the uncertainties. You need an absorption correction if you are dealing with light elements, with K lines <1 keV. Under these circumstances, the extrapolation technique of Horita *et al.* is the best approach; a detailed example of the determination of light-element k factors using this method has been given by Westwood *et al.* (1992). Further refinements of Horita's method have been proposed by Eibl (1993). In the specific case of ionic compounds in which electroneutrality must be maintained (i.e., the sum of all anions and cations, times their valence states, must balance), it is even possible to devise an absorption correction with no estimate of t (Van Cappellen and Doukhan 1994).

35.7. THE FLUORESCENCE CORRECTION

X-ray absorption and fluorescence are intimately related because the primary cause of X-ray absorption is the fluorescence of another X-ray (such as the fluorescence of Si K_α X-rays in the XEDS detector which gives rise to the escape peak). You might think, therefore, that fluorescence corrections should be as widespread as absorption corrections. However, this is not the case for the following reasons. Strong absorption effects occur when there is a small amount of one element whose X-rays are being absorbed by the presence of a relatively large amount of another element. The absorption of Al K_α X-rays by Ni in Ni_3Al is a classic example. In this case, Ni X-rays are indeed fluoresced as a result of the absorption of Al K_α X-rays. However, there is a relatively small increase in the total number of Ni X-rays because Ni is the dominant element; the relative decrease in the Al K_α intensity is large because Al is the minor constituent. In this particular example there is a further reason why fluorescence of Ni X-rays is ignored; it is the Ni L_α X-rays which are fluoresced by the absorption of Al K_α X-rays. The Ni L X-rays are not the ones that we use for microanalysis anyhow, since the higher-energy Ni K X-rays are not absorbed or fluoresced.

Fluorescence is usually a minor effect and often occurs for X-rays that are not of interest.

However, in the rare case that fluorescence occurs to a degree that limits the accuracy of microanalysis, the equation used for the fluorescence correction factor (FCF) is that developed by Nockolds *et al.* (1980); a detailed discussion is given by Anderson *et al.* (1995). Practical examples of the fluorescence correction are hard to come by and the classic case is Cr in stainless steels, where the Cr K_α line is fluoresced by the major peak, the Fe K_α line, giving rise to an increase in apparent Cr content as the foil gets thicker. You can also avoid the problem of thickness measurement for fluorescence corrections, just as for absorption, using a similar parameterless correction (Van Cappellen 1990).

35.8. ALCHEMI

We told you early on in this chapter to take your X-ray spectra away from strong diffraction conditions. This is because of the "Borrmann effect." As we saw back in Sections 13.8, 13.9, and 14.6, close to two-beam conditions the Bloch waves interact strongly with the crystal planes, and so X-ray emission is enhanced compared with kinematical conditions, as shown in Figure 35.11A. Now we can make use of this phenomenon to locate which atoms lie on which crystal planes. The technique has the delightful (and wholly inappropriate) acronym ALCHEMI, which is a selective abbreviation of the expression "Atom Location by CHanneling-Enhanced MIcroanalysis."

ALCHEMI is a quantitative technique for identifying the crystallographic sites, distribution, and types of substitutional impurities in many crystals. The technique was first developed for the TEM by Spence and Taftø (1983), who coined the acronym. The derivation of the quantitative expressions that we give below follows that paper. Channeling is widely used for atom site location in other analysis techniques (e.g., see Chu *et al.* 1978).

The way to do ALCHEMI experimentally is to acquire a spectrum under strong channeling conditions, such that the Bloch wave is interacting strongly with a particular systematic row of atoms. This channeling orientation should be chosen so that the planes interacting strongly with the electron beam also contain the candidate impurity atom sites, so you must have some *a priori* ideas about where substitutional atoms are most likely to sit. This technique is therefore particularly well suited to layer structures. When the Bloch wave is maximized on a particular plane of atoms, the X-ray intensity from the atoms in that

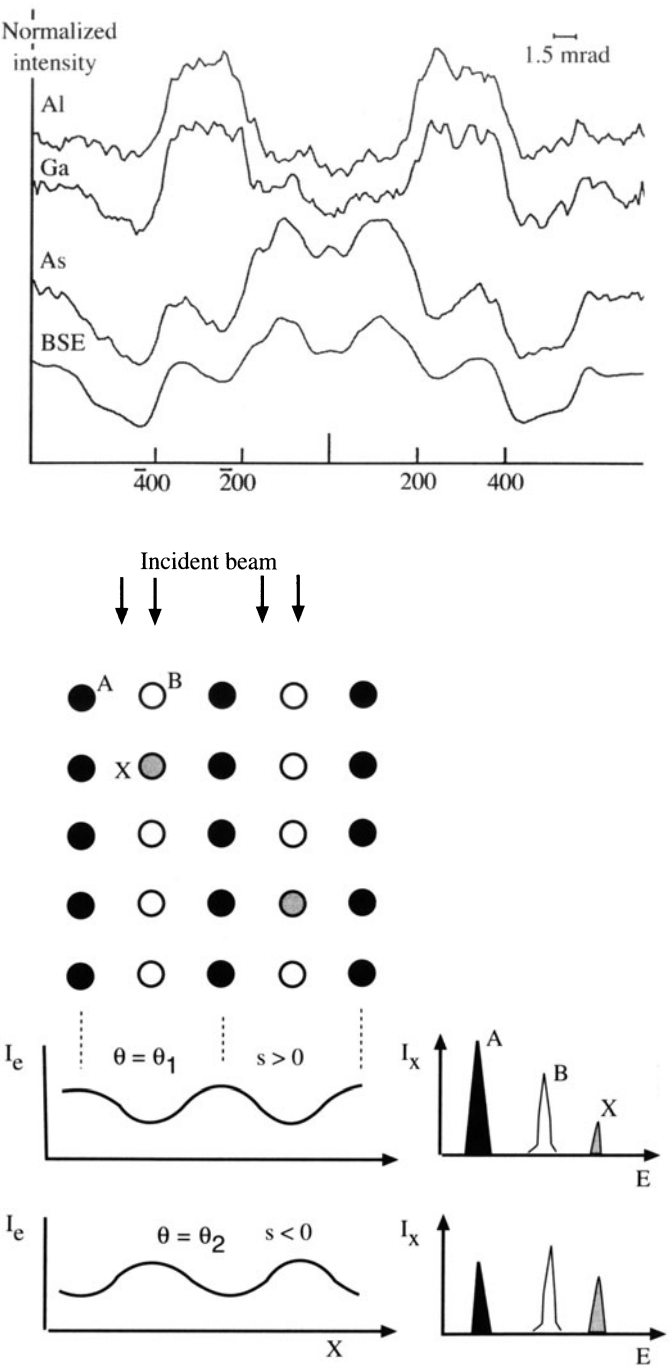

Figure 35.11. (A) The Borrmann effect: the variation in characteristic X-ray emission close to strong two-beam conditions as the beam is rocked across the 400 planes of GaAlAs. The X-rays from Al, which occupies Ga sites, follow the Ga X-ray emission while the As varies in an approximately complementary fashion. The backscattered electron signal (BSE) is inversely proportional to the amount of electron channeling, so the As signal is strongest where the channeling is weakest. (B) ALCHEMI allows the determination of the site occupancy of atom X in columns of atoms A and B. By tilting to $\mathbf{s} > 0$ and $\mathbf{s} < 0$, the Bloch waves interact strongly with row A and then row B, giving different characteristic intensities shown schematically in the spectra, from which the relative amounts of X in columns of A and B can be determined.

plane will be highest. Start by finding the orientations that give the most pronounced channeling effects for the atoms *A* and *B*, as shown schematically in Figure 35.11B. Usually a very small tilt is all that is necessary to get a different spectrum.

If you are looking at two elements, *A* and *B*, and a substitutional element *X*, follow this procedure:

- Measure X-ray intensities from each element in orientations 1 and 2.
- Then find a nonchanneling orientation (3) where electron intensity is uniform for both planes.

In this orientation we define the ratio *k* as

$$k = \frac{I_B}{I_A} \qquad [35.36]$$

where I_B is the number of X-ray counts from the element *B* in the nonchanneling orientation. For the two channeling orientations 1 and 2, we define two parameters β and γ such that

$$\beta = \frac{I_B^{(1)}}{k\, I_A^{(1)}} \qquad [35.37]$$

and

$$\gamma = \frac{I_B^{(2)}}{k\, I_A^{(2)}} \qquad [35.38]$$

Now assuming we know that the element *X* sits on specific sites, say it substitutes for atom *B*, then we define an intensity ratio term *R* such that

$$R = \frac{I_A^{(1)}\, I_X^{(2)}}{I_X^{(1)}\, I_A^{(2)}} \qquad [35.39]$$

Hence the fraction of atom *X* on *B* sites is given by

$$C_X = \frac{R - 1}{R - 1 + \gamma - \beta R} \qquad [35.40]$$

Similar expressions can be generated for *X* atoms on *A* sites, but in fact the fraction of *X* atoms on *A* sites must be $1 - C_X$.

As you see, ALCHEMI can give a direct measure of the occupation of substitutional sites. However, the intensity differences in different orientations are often quite small and you need good X-ray statistics to draw sound conclusions. This makes it difficult to apply if high spatial resolution is also desired because, as we shall see in the next chapter, the conditions to give the best spatial resolution also give the worst counting statistics.

35.9. EXAMPLES; PROFILES AND MAPS

The best way to appreciate the value of quantitative analysis is to go and study some applications. In Figure 35.12, composition data from a complex three-component Ni-Cr-Mo high-temperature superalloy are plotted to reveal a section of the ternary phase diagram (Raghavan *et al.* 1984).

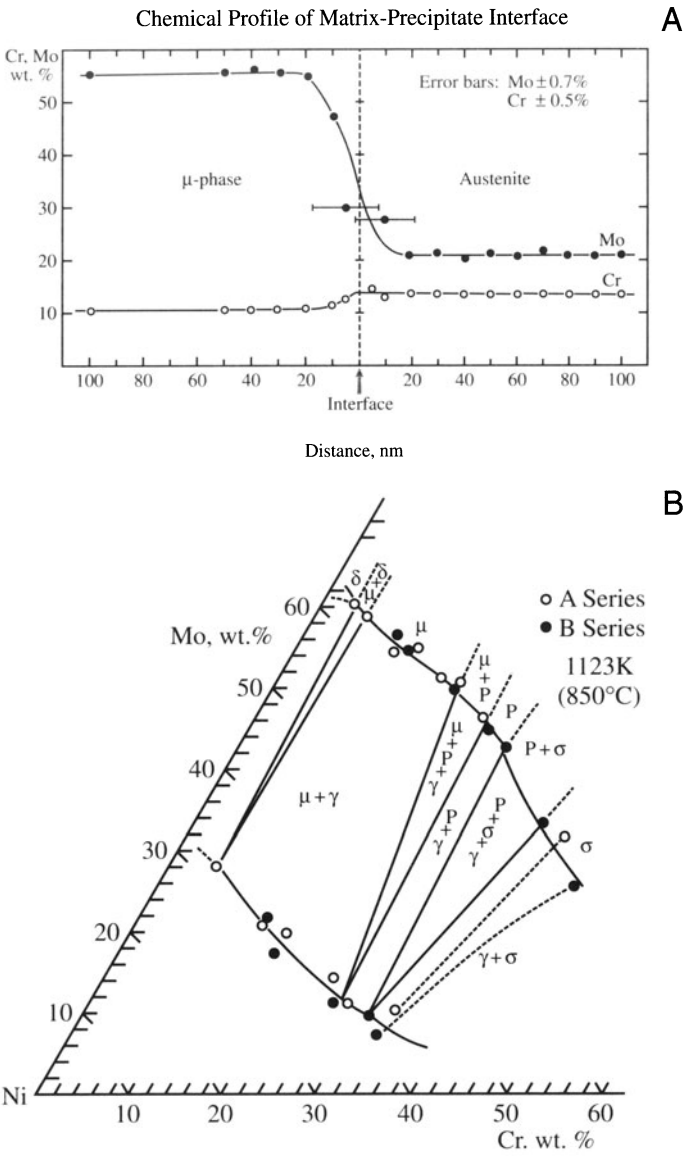

Figure 35.12. (A) Cr and Mo composition profiles across a two-phase μ–γ interface in a Ni-10Cr-30Mo alloy which has been aged 1000 hr at 1123 K. The profiles show composition changes that define tie lines in the ternary phase diagram. (B) A corner of the Ni-Cr-Mo ternary phase diagram determined by XEDS microanalysis of thin foils of heat-treated specimens containing up to three phases. The limits of the undesirable σ–phase regions are the important phase boundaries in this material.

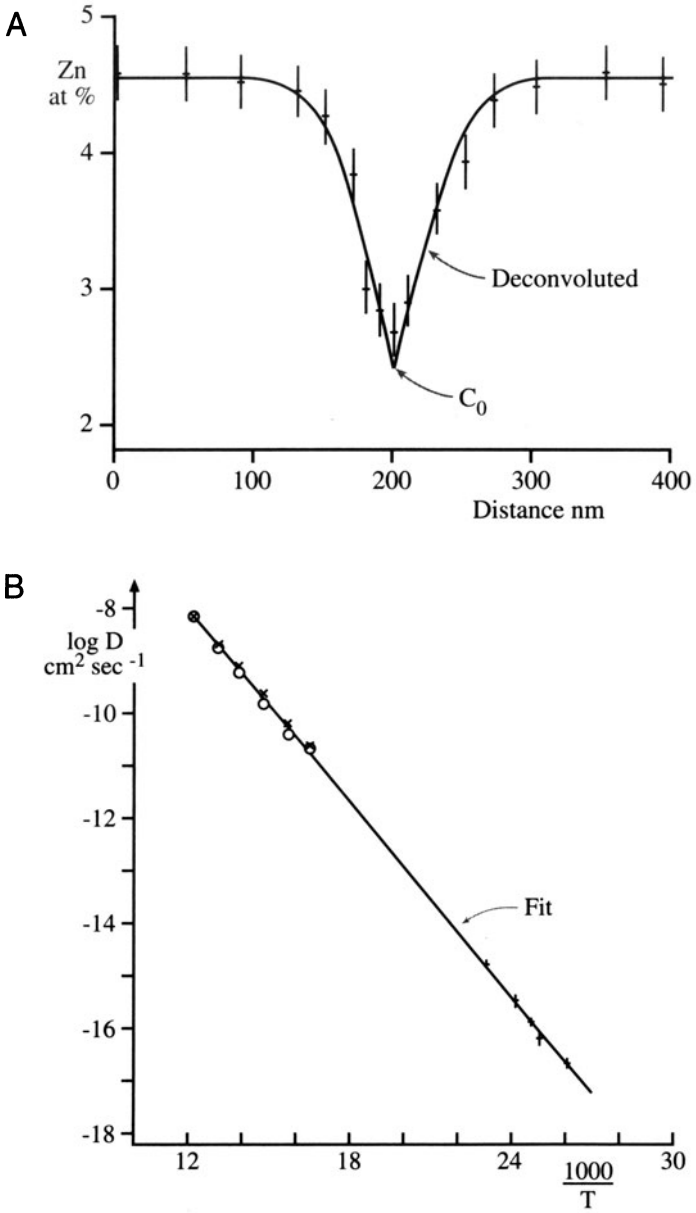

Figure 35.13. (A) Zn concentration profile across a grain boundary in an Al-4.5 at.% Zn alloy aged at 125°C to produce a solute-depleted region due to equilibrium grain boundary precipitation. Grube analysis of the profiles give a measure of D. The low aging temperatures produce such small profiles that AEM is the only way to measure them. (B) Arrhenius plot of the diffusivity of Zn in Al, as a function of temperature, derived from measurements of Zn composition profiles in (A). Extrapolation of high-temperature diffusion data match up well with the AEM results.

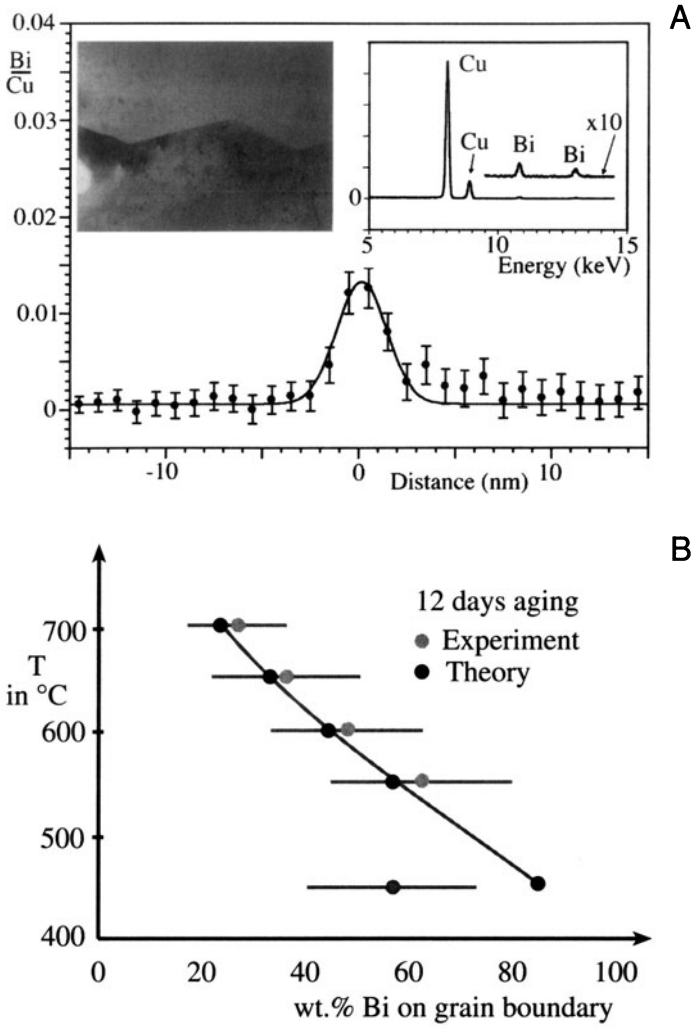

Figure 35.14. (A) XEDS measurements of the distribution of Bi segregated to a grain boundary in Cu. A faceted Cu GB, typical of those to which Bi is segregated, is shown in the upper-left inset and an XEDS spectrum from the GB region in the upper right reveals small Bi peaks. (B) Quantification of similar Bi spectra to that in (A) shows an inverse relationship with temperature, consistent with classical McLean adsorption isotherm predictions, shown as the fitted line.

Assuming interface equilibrium, sections such as the three-phase triangle can be measured from a single thin foil. In this study the undesirable σ–phase boundaries were sought, to avoid embrittlement of the alloy in service. In Figure 35.13, solute profiles measured across grain boundaries in Al-Zn (Nicholls and Jones 1983) permitted measurement of the diffusion coefficient of Zn in Al to much lower temperatures than previously attained with traditional EPMA methods. In Figure 35.14, the detection of Bi equilibrium segregation to grain boundaries in Cu is modeled by a simple McLean-type adsorption isotherm (Michael and Williams 1984). Previous studies of such Gibbsian segregation required *in situ* fracture of embrittled Cu inside Auger spectrometer systems.

We should also note that individual point analysis, or profiles across an interface, are not the only way to display X-ray data. It is possible to produce X-ray images or maps in which the intensity of the signal in the map is directly related to the X-ray intensity I_A. In a quantitative

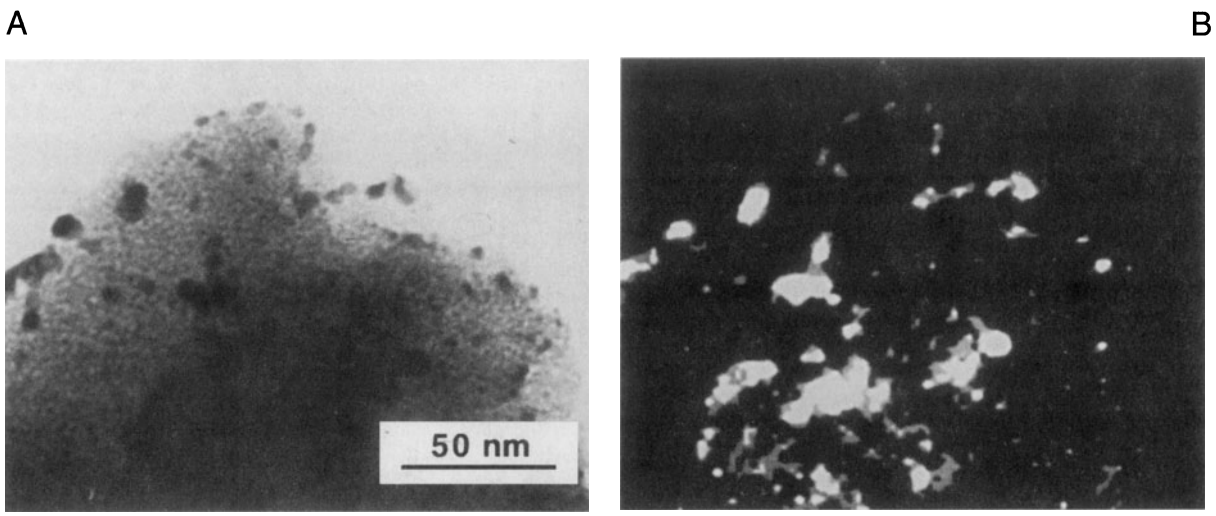

Figure 35.15. (A) BF STEM image of PD catalyst particles on a carbon support film. (B) Qualitative Pd L_α X-ray image of the distribution of Pd.

map, the X-ray signal is proportional to the concentration C_A. While there are obvious advantages to comparing quantitative maps of elemental distributions with other TEM images, this process is limited by the relatively poor statistics of X-ray acquisition. Remember that good quantification requires ~10,000 counts for I_A. Even in an efficient AEM, this intensity may easily take one minute to acquire. At this acquisition rate, even a 56 × 56 pixel image will take 50 hours to gather, so it is impractical. We need to increase the efficiency of X-ray acquisition markedly, or we just have to make do with qualitative, noisy maps, as shown in Figure 35.15, even when using an FEG-AEM.

CHAPTER SUMMARY

Quantitative microanalysis of spectra from thin foils is straightforward in most cases, so long as you take care to determine the *k* factors with sufficient accuracy. The software to handle the more difficult problem of absorption is well known and commercially available. Perhaps the greatest difficulty remains the need to know the specimen thickness in order to compensate for X-ray absorption, and extrapolation techniques are invaluable in avoiding this. We can minimize absorption by making the thinnest possible specimens, but then the possibility arises that the number of X-ray counts may be so small that errors in the quantification are large. The use of FEG sources and improved TEM-EDS configurations to maximize the collection angle will help in this situation.

REFERENCES

General References

Goldstein, J.I. (1979) in *Introduction to Analytical Electron Microscopy* (Eds. J.J. Hren, J.I. Goldstein, and D.C. Joy), p. 83, Plenum Press, New York.

Goldstein, J.I., Williams, D.B., and Cliff, G. (1986) in *Principles of Analytical Electron Microscopy* (Eds. D.C. Joy, A.D. Romig, and J.I. Goldstein), p. 155, Plenum Press, New York.

Romig A.D. Jr. (1986) *Analytical Transmission Electron Microscopy,* Metals Handbook, 9th edition, **10**, p. 429, American Society for Metals, Metals Park, Ohio.

Williams, D.B. (1987) *Practical Analytical Electron Microscopy in Materials Science,* 2nd edition, Philips Electron Optics Publishing Group, Mahwah, New Jersey.

Williams D.B. and Goldstein J.I. (1991) in *Electron Probe Quantitation* (Eds. K.F.J. Heinrich and D.E. Newbury), p. 371, Plenum Press, New York.

Zaluzec, N.J. (1979) in *Introduction to Analytical Electron Microscopy* (Eds. J.J. Hren, J.I. Goldstein, and D.C. Joy), p. 121, Plenum Press, New York.

Specific References

Anderson, I.M., Bentley, J., and Carter, C.B. (1995) *J. Microsc.* **178**, 226.

Bambynek, W., Crasemann, B., Fink, R.W., Freund, H.U., Mark, H., Swift, C.D., Price, R.E., and Rao, P.V. (1972) *Rev. Mod. Phys.* **44**, 716.

Bender, B.A., Williams, D.B., and Notis, M.R. (1980) *J. Am. Ceram. Soc.* **63**, 149.

Castaing, R. (1951) Thesis, University of Paris, ONERA Publication, #55.

Chapman, J.N., Nicholson, W.A.P., and Crozier, P.A. (1984), *J. Microsc.* **136**, 179.

Chu, W.-K., Mayer, J.M., and Nicolet, M.-A. (1978) *Backscattering Spectrometry,* Academic Press, Orlando, Florida.

Cliff, G. and Lorimer, G.W. (1975) *J. Microsc.* **103**, 203.

Eibl, O. (1993) *Ultramicrosopy* **50**, 179.

Goldstein, J.I., Costley, J.L., Lorimer, G.W., and Reed, S.J.B. (1977) *SEM 1977,* **1** (Ed. O. Johari), p. 315, IITRI, Chicago, Illinois.

Graham, R.J. and Steeds, J.W. (1984) *J. Microsc.* **133**, 275.

Heinrich, K.F.J. (1986) in *Proc. ICXOM-11* (Eds. J. Brown and R. Packwood), p. 67, University of Western Ontario, Canada.

Heinrich, K.F.J. and Newbury, D.E., Eds. (1991) *Electron Microprobe Quantitation,* Plenum Press, New York.

Hillier, J. and Baker, R.F. (1944) *J. Appl. Phys.* **15**, 663.

Horita, Z., Sano, T., and Nemoto, M. (1987) *Ultramicroscopy* **21,** 271.

Kramers, H.A. (1923) *Phil. Mag.* **46**, 836.

Lorimer, G.W., Al-Salman, S.A., and Cliff, G. (1977) in *Developments in Electron Microscopy and Analysis* (Ed. D.L. Misell), p. 369, The Institute of Physics, Bristol and London.

McGill, R.H. and Hubbard, F.H. (1981) in *Quantitative Microanalysis with High Spatial Resolutions* (Eds. G.W. Lorimer, M.H. Jacobs, and P. Doig), p. 30, The Metals Society, London.

Michael, J.R. and Williams, D.B. (1984) *Met. Trans.* **15A**, 99.

Nicholls, A.W. and Jones, I.P. (1983) *J. Phys. Chem. Solids* **44**, 671.

Nockolds, C., Nasir, M.J., Cliff, G., and Lorimer, G.W. (1980) in *Electron Microscopy and Analysis-1979* (Ed. T. Mulvey), p. 417, The Institute of Physics, Bristol and London.

Owen, D.B. (1962) *Handbook of Statistical Tables,* Addison-Wesley, Reading, Massachusetts.

Powell, C.J. (1976) in *Use of Monte Carlo Calculations in Electron Probe Microanalysis and Scanning Electron Microscopy* (Eds. K.F.J. Heinrich, D.E. Newbury, and H. Yakowitz), p. 61, U.S. Department of Commerce/NBS, Washington, DC.

Raghavan, M., Mueller, R.R., Vaughn, G.A., and Floreen, S. (1984) *Met. Trans.* **15A**, 783.

Schreiber, T.P. and Wims, A.M. (1981) *Ultramicroscopy* **6**, 323.

Schreiber, T.P. and Wims, A.M. (1982) *X-ray Spectrometry* **11**, 42.

Sheridan, P.J. (1989) *J. Electr. Microsc. Tech.* **11**, 41.

Spence, J.C.H. and Taftø, J. (1983) *J. Microsc.* **130**, 147

Sprys, J.W. and Short, M.A. (1976) *Proc. 34th EMSA Meeting* (Ed. G.W. Bailey), Claitors, Baton Rouge, Louisiana.

Van Cappellen, E. (1990) *Microsc. Microanal. Microstruct.* **1**, 1.

Van Cappellen, E. and Doukhan, J.C. (1994) *Ultramicroscopy* **53**, 343.

Westwood, A.D., Michael, J.R., and Notis, M.R. (1992) *J. Microsc.* **167**, 287.

Williams, D.B. and Goldstein, J.I. (1991) in *Electron Probe Quantitation* (Eds. K.F.J. Heinrich and D.E. Newbury), p. 371, Plenum Press, New York.

Williams, D.B., Newbury, D.E., Goldstein, J.I., and Fiori, C.E. (1984) *J. Microsc.* **136**, 209.

Wood, J.E., Williams, D.B., and Goldstein, J.I. (1981) in *Quantitative Microanalysis with High Spatial Resolutions* (Eds. G.W. Lorimer, M.H. Jacobs, and P. Doig), p. 24, The Metals Society, London.

Wood, J.E., Williams, D.B., and Goldstein, J.I. (1984) *J. Microsc.* **133**, 255.

Zaluzec, N.J., Maher, D.M., and Mochel, P.E. (1981) in *Analytical Electron Microscopy-1981* (Ed. R.H. Geiss), p. 25, San Francisco Press, San Francisco, California.